In situ vapor sorption apparatus for small-angle neutron scattering and its application

Man-Ho Kim[a)]
National Institute of Standards and Technology (NIST) Center for Neutron Research, National Institute of Standards and Technology, Gaithersburg, Maryland 20899-8562 and Department of Materials Science and Engineering, University of Maryland, College Park, Maryland 20742-2115

Charles J. Glinka
National Institute of Standards and Technology (NIST) Center for Neutron Research, National Institute of Standards and Technology, Gaithersburg, Maryland 20899-8563

Robert N. Carter
General Motors Corporation, Fuel Cell Activities, 10 Carriage Street, P.O. Box 603, Honeoye Falls, New York 14472-0603

(Received 19 July 2005; accepted 10 October 2005; published online 21 November 2005)

An *in situ* vapor sorption apparatus has been constructed for use in small-angle neutron scattering (SANS) measurements. The apparatus adapts two independent operating mechanisms, with and without a carrier gas, to control relative or absolute pressure, respectively, in the SANS sorption cell. By controlling the absolute pressure, a target relative vapor pressure between 0% and 90% can be reached within 1–2 min. The short response time makes it possible to correlate diffusion kinetics and/or sorption/desorption isotherms with structure evolution during wetting/drying, which is not possible in gravimetric methods. Also, one can extract diffusion coefficients and interaction parameters. Other uses include the enhancement of scattering contrast in the study of semicrystalline polymers by the preferential vapor sorption of deuterated vapor into the amorphous regions. Thus, one can obtain the same structural information as small-angle x-ray scattering measurements on dry samples. Also, the apparatus has the capability to inject a pore-masking liquid into the sample cell while under vacuum to ensure the filling of all open porosities in a sample. The capability to mix two vapors in various ratios facilitates the determination of a contrast-matching point using a single sample, which also eliminates a major source of systematic error. The performance of the apparatus is demonstrated using a polyelectrolyte membrane and semicrystalline polyethylene. Additionally, technical points relating to controlling the relative vapor pressure, relative humidity, and regarding the vapor distribution in the cell are discussed. © *2005 American Institute of Physics.*
[DOI: 10.1063/1.2134151]

I. INTRODUCTION

Small-angle neutron scattering (SANS) has been used to study structures with length scales of 10–5000 Å for various materials systems such as polymer blends, porous materials, membranes, colloids, gels, and composites. A fundamental requirement for small-angle scattering (SAS) is scattering contrast across interfaces in the sample. The capability for controlling contrast is a pivotal factor in scattering experiments. If the contrast is not strong enough, the scattering may be negligible. In addition, if the system contains voids (or trapped air), the scattering from voids may obscure the scattering from the structure of interest. One of the unique features of neutron scattering is the relative ease in varying scattering contrast. Scattering from a particular structure can, for example, be made visible by reducing the contrast from other structures with an appropriate mixture of hydrogenated(H)/deuterated(D) solvents.

The purpose of this study was to develop a multipurpose apparatus for SANS experiments (as well as wide angle x-ray scattering and infrared spectroscopy) that enables one to (i) control vapor pressure or relative humidity accurately and quickly, (ii) perform contrast-matching and/or -enhancing experiments by mixing vapors of solvents, (iii) and absorb liquid into a porous sample under vacuum. Controlling these experimental parameters easily will advance the experimental and theoretical study of, for example:

- semicrystalline polymers, which typically lack neutron-scattering contrast, by selective wetting of the amorphous phase,
- pore size distributions based on Kelvin capillary condensation theory,
- and ionic group aggregation in polyelectrolyte membranes.

Several vapor sorption control methods have been used in various scientific fields: (i) in SANS by Hoinkis[1] and by Hedden *et al.*[2] with pressure and flow rate control methods,

[a)]Author to whom correspondence should be addressed; electronic mail: man-ho.kim@nist.gov

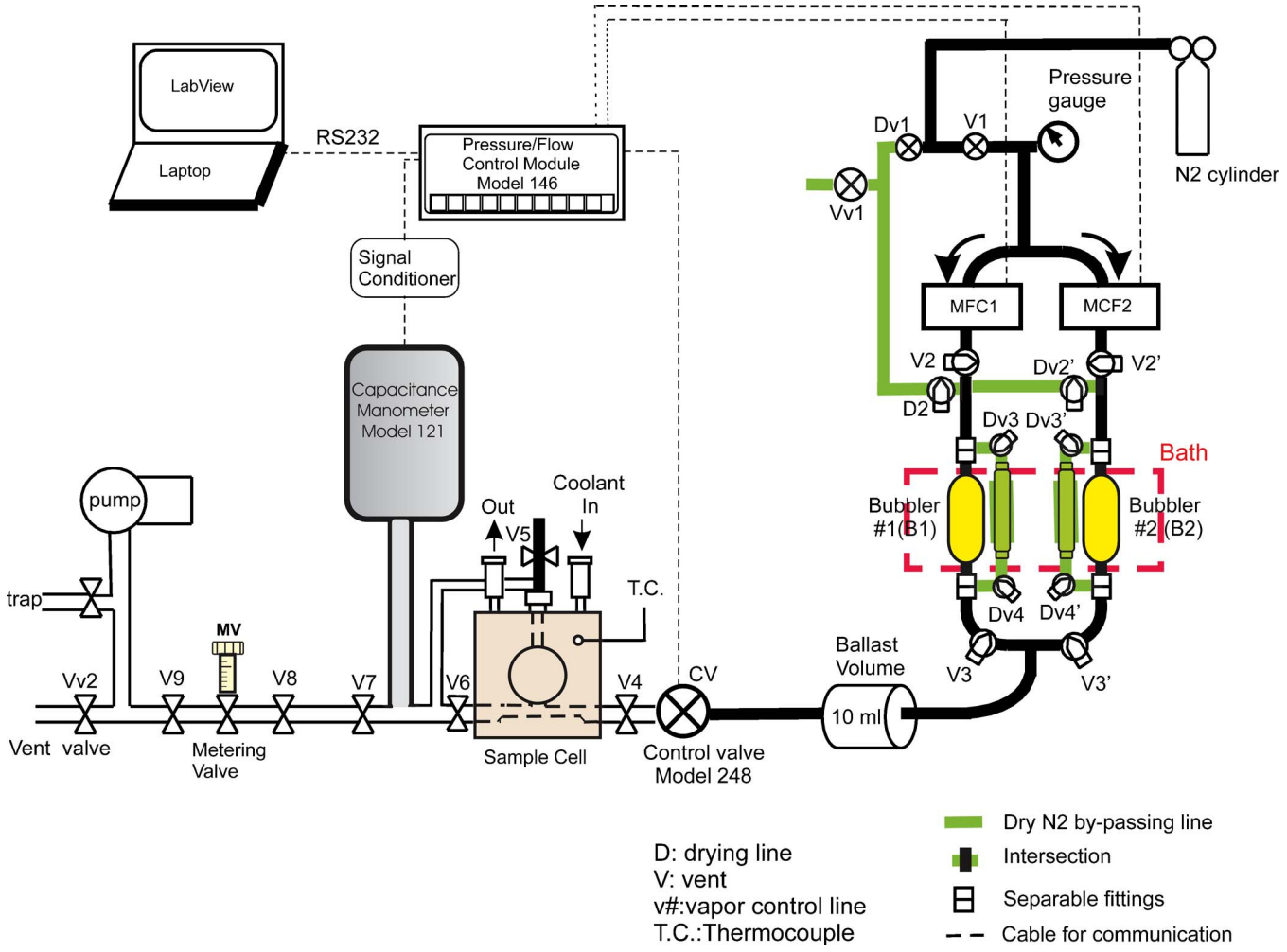

FIG. 1. Schematic of *in situ* vapor sorption apparatus.

respectively, (ii) in x-ray reflection by Soles *et al.*[3] with both flow and pressure control methods, (iii) in chemical-vapor deposition area by Hersee and Ballingall[4] and by Kondoh and Ohta[5] with simultaneous control of the pressure and flow rate, (iv) in vapor sorption by Dhoot and Freeman[6] with flow rate control, and (v) in humidity control with two pressure controls.[7] Various humidity control methods have been reviewed in Ref. 8.

The overall schematics and individual components of the apparatus are described in Sec. II and the principles of controlling vapor pressure are described in Sec. III. The method and capability for controlling relative humidity using the present *in situ* vapor sorption apparatus are described in detail in Sec. IV. Finally, some preliminary experimental results are presented in Sec. V to demonstrate the performance of the apparatus.

II. DESCRIPTION OF *IN SITU* VAPOR SORPTION APPARATUS

The apparatus consists of four parts: vapor generator, vapor delivery line, sample compartment, and control module. An overall schematic is shown in Fig. 1. The vapor is generated by flowing a dry carrier gas through two bubblers. The carrier gas flow rate is controlled by the mass flow controllers (MFC) located upstream of the bubblers. The dry gas and vapor delivery lines are stainless steel of outer diameter (o.d.)=1.6 mm [inner diameter (i.d.)≅0.8 mm], and copper of o.d.=3.1 mm (i.d.≅1.6 mm), respectively. Copper is used for better heat conduction and the larger diameter provides a larger reservoir and less flow resistance. A 10 ml cylinder is located downstream from the bubblers to facilitate mixing of the two streams. The control system consists of two mass flow controllers (MKS Model: 1479A) (NIST disclaimer),[9] a control valve (MKS Model: 248), a capacitance manometer (MKS: 121A), a Control Module (MKS: 146C), and a personal computer (PC). Metal seals were used for the MFC and Kalrez perfluoroelastomers seals for the control valve to avoid malfunctioning of the part due to swelling of the conventional rubber O-rings by organic solvent vapor. This system enables (i) mixing two vapors in a desired molar ratio by controlling the carrier gas flow rate of each bubbler with dedicated mass flow controllers; (ii) dilution of the saturated vapor from one bubbler using a diluent dry gas; and (iii) control of the vapor pressure in the sample compartment using the capacitance manometer and control valve. The following are detailed descriptions of each part of the *in situ* vapor sorption apparatus.

A. Bubbler

The bubbler (Aldrich in-line oil bubbler) is a glass container that one partially fills with liquid to submerge a sparger (i.e., porous cap) on the end of a gas inlet tube. The sparger produces a stream of fine bubbles to more easily saturate the carrier gas. The bubbler was modified to have three tube arms made of Kovar alloy for carrier gas inlet, saturated vapor outlet, and liquid loading. (Corrosion of Kovar alloy tested at various water temperatures was not observed.) The bubbler temperature is controlled by immersion in a recirculating bath. The working volume of the bubbler is approximately 5 ml.

B. Vapor delivery lines

The two bubblers are located at some distance from the sample compartment due to space limitations in the SANS instrument and safety considerations. The copper tubing (inner diameter $\cong 1.6$ mm) that delivers vapor to the sample cell is wrapped with heating tape to prevent condensation in the lines. Using a larger diameter tubing has the advantage of minimizing the pressure drop (see the Appendix). However, when an expensive deuterated solvent is used, increasing the vapor delivery tubing diameter may become a disadvantage. One end has a quick connect fitting to the control valve. All vapor delivery lines, vapor delivery tube, volume ballast cylinder, control valve, capacitance manometer, and sample cell compartment as well as a vacuum line can be heated to dry the system if necessary.

C. Control system

There are two main control methods: (1) vapor flow rate control upstream of the sample cell, and (2) pressure control in the sample cell. Both vapor flow and pressure are controlled by the same control module. Mixing vapor for a desired mole fraction is performed by controlling each carrier gas flow rate through two mass flow controllers. Also, the vapor pressure in the sample cell can be controlled by the control valve using pressure feedback from the capacitance manometer. The metering valve downstream of the sample cell further modulates the pressure in the cell by controlling gas flow to the vacuum pump.

D. Sample cell design

The sample cell is made from titanium (grade 2) to accommodate samples up to 25.4 mm in diameter and variable thickness between 1.0 and 5.0 mm. Titanium was chosen because it has reasonably good corrosion resistance and does not become activated by neutron capture. Samples are loaded by removing one of the transparent (to both visible light and neutrons) beam windows (thickness: 1.0 mm), made from Supracil-grade silica or its equivalent. The cell is designed to control the sample temperature over a range from 0 °C to (150 ± 0.5) °C by a combination of heating rope and recirculating water bath. Also the cell is designed to withstand an internal pressure up to 350 kPa and maintain a vacuum of 10^{-4} kPa. The helium leak rate was measured with a mass spectrometer to be 10^{-5} kPa cm^3/s. When under vacuum the entire system was found to loose vacuum at a rate of

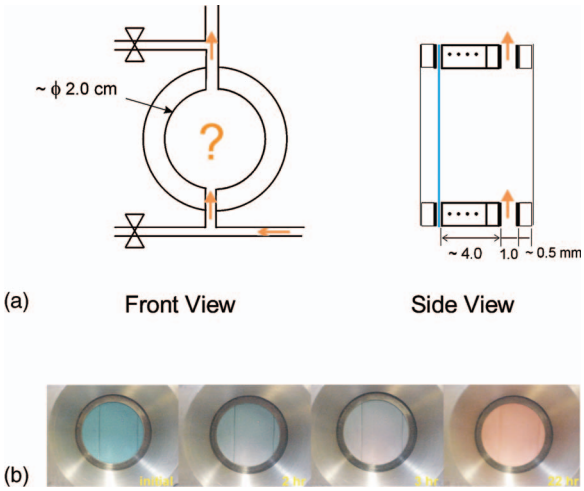

FIG. 2. (Color) Sample cell design: (a) two-hole setup and (b) color change of humidity indicator paper with vapor wetting time.

0.13 Pa/h (10^{-3} Torr/h), which may be due to a virtual leak (i.e., a leak of air or vapor trapped in the screw threads of sample retainer or fittings) rather than an external leak or the sum of equivalent small leaks from all fittings. This leak does not affect vapor pressure control below the saturated vapor pressure as long as a leak rate is smaller than vapor delivery rate into the cell because the pressure in the cell is dynamically controlled. However, it does make it difficult to measure a saturated vapor pressure. The cell window retainer on the exit side has a conical taper to allow scattering up to ±25° to be unobstructed.

E. Vapor distribution in the sample cell

The distribution of vapor in the entire cell volume must be homogeneous to wet the sample uniformly, and thereby prevent any nonhomogeneous structure evolution. In order to check the vapor distribution in the sample cell, pieces of blue humidity indicator paper (cobalt chloride paper, 0.2 mm thick) were attached on both sides of a piece filter paper (total thickness around 0.6 mm) placed in the cell and wetted using water vapor carried by nitrogen gas. Two different cell designs were tested: one with holes at the bottom and top (Fig. 2) and another using a spacer with six holes (Fig. 3). If the vapor in the cell distributes evenly, the color of the humidity indicator paper is expected to change uniformly from blue to pink without any color gradient. The paper was placed at a distance of 4 mm from the vapor inlet orifice in order for the vapor to have a better chance to distribute uniformly in the space before touching the paper. As shown in Fig. 2, the two-hole system shows two distinct colors until 50% relative humidity (RH), pink for the bottom and blue for the top, indicating that the vapor wet the bottom part first, while the entire paper showed a uniform pink color when the saturation point was reached. This nonuniform distribution of vapor was overcome by using the spacer (Fig. 3) with six holes connected to a circular channel. (The bottom hole size was around 0.3 mm in diameter while the rest were approximately 1.0 mm.) The cobalt chloride paper showed a uniform color change with wetting time, demonstrating that uniform distribution of the water vapor in the cell was achieved with

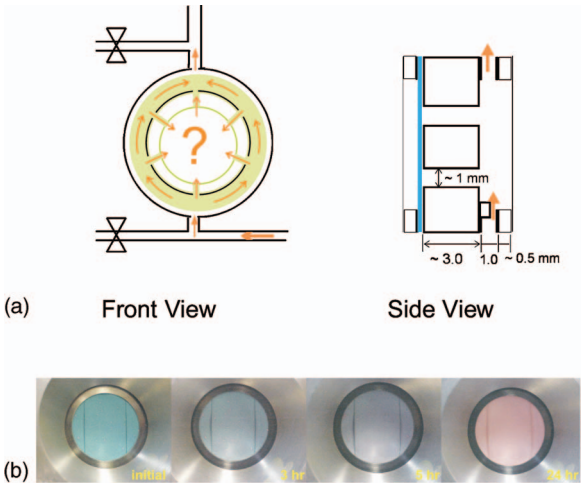

FIG. 3. (Color) Sample cell design: (a) six-hole setup and (b) color change of humidity indicator paper with vapor wetting time.

the special spacer. In the next section, operational principles and background theory for controlling the vapor pressure are discussed.

III. PRINCIPLES OF OPERATIONS

The apparatus is operated with one of two modes: flow rate control (open-loop operation) and pressure control (pseudoclosed-loop operation). Flow rate control is used for (i) mixing two vapors and (ii) diluting saturated vapor, while pressure control is used to deliver vapor to the cell with a target vapor pressure without a carrier gas. The principles of these modes of operation are listed in Fig. 4 and described below.

A. Delivery of saturated vapor with a single bubbler and carrier gas

This mode is used when a sample is to be exposed to a saturated vapor environment. Only one mass flow controller and a carrier gas are used. A simplified schematic of this operation is shown in Fig. 4(a). Carrier gas is delivered by a MFC1 at a programmed flow rate, $F_{1,c}$ (in SCCM; standard cm^3/min), and flows into the bubbler, B1. This gas is saturated with solvent vapor in the bubbler. The molar fraction ($\phi^*_{1,v}$) of the saturated vapor in the gas mixture exiting the bubbler is

$$\phi^*_{1,v} = \frac{P^*_{1,v}}{P_{1,T}} = \frac{F^*_{1,v}}{F_{1,c} + F^*_{1,v}}, \tag{1}$$

where $P^*_{1,v}$ is the saturated vapor pressure of the liquid at the temperature of B1, and $P_{1,T}$ is the total pressure in the bubbler as measured by the pressure transducer at the bubbler.[10] (The subscripts, c, v, T, and superscript * stand for carrier gas, vapor, total, and saturated vapor, respectively). The saturated vapor flow rate in B1 is given by

$$F^*_{1,v} = \frac{\phi^*_{1,v} F_{1,c}}{(1 - \phi^*_{1,v})}. \tag{2}$$

B. Delivery of mixed vapor with two bubblers and carrier gas

One of the advantages of neutron scattering over other radiation scattering methods is the ability to use contrast matching to discriminate among different domains (or phases) in a mixed domain system. In a neutron-scattering experiment, contrast variation is obtained by simply exposing the sample to mixtures of protonated and deuterated forms of water or organic solvent. The *in situ* vapor sorption apparatus can mix two gas streams to a desired ratio using two bubblers, B1 and B2, and two MFCs, MFC1, and MFC2 as illustrated in Fig. 4(b).

1. Exact mass balance

Regardless of whether the saturated partial vapor pressure is the same or different for the two fluids, the molar fraction, $\phi_{1,v}$, of vapor 1 in the mixture can be expressed as

$$\phi_{1,v} = \frac{F^*_{1,v}}{F_{1,T} + F_{2,T}} = \frac{F_{1,T}\phi^*_{1,v}}{F_{1,T} + F_{2,T}}, \tag{3}$$

where $F_{1,T} = F_{1,c} + F^*_{1,v}$. The total flow rates from each bubbler are given by

$$F_{1,T} = \frac{F_{1,c}}{1 - \phi^*_{1,v}}, \quad F_{2,T} = \frac{F_{2,c}}{1 - \phi^*_{2,v}}. \tag{4}$$

Thus, $\phi_{1,v}$ can be expressed in terms of the flow rates of the carrier gas and the saturated molar fractions

$$\phi_{1,v} = \frac{F_{1,c}\phi^*_{1,v}/(1 - \phi^*_{1,v})}{F_{1,c}/(1 - \phi^*_{1,v}) + F_{2,c}/(1 - \phi^*_{2,v})}. \tag{5}$$

2. Approximate mass balance

If both liquids have vapor pressures that are small compared with the corresponding carrier gas partial pressure, $P^*_{1,v} \ll P_{1,c}$ and $P^*_{2,v} \ll P_{2,c}$, $\phi^*_{1,v}$ and $\phi^*_{2,v}$ can be neglected at each denominator of Eq. (5). Thus, Eq. (5) can be approximated as

$$\phi_{1,v} \cong \frac{F_{1,c}}{F_{1,c} + F_{2,c}} \phi^*_{1,v}. \tag{6}$$

This requires knowing only the two flow rates of the carrier gas because $\phi^*_{1,v}$ is constant at a given temperature.

C. Relative vapor pressure control

1. Flow rate (open loop) control

Two MFCs allow one to control relative vapor pressure in the sample cell by diluting the saturated vapor flowing out from B1 with the diluent gas from the dry B2 as shown in Fig. 4(c). When the saturated vapor from the bubble 1 is mixed with a diluent gas (for example, dry N_2 gas), the diluted vapor mole fraction is given by

$$\phi^{\text{diluted}}_{1,v} = \frac{F^*_{1,v}}{F_T}, \tag{7}$$

where $F_T = F_{1,T} + F_{2,\text{diluent}}$.

Combining Eq. (7) with Eqs. (2) and (4) gives

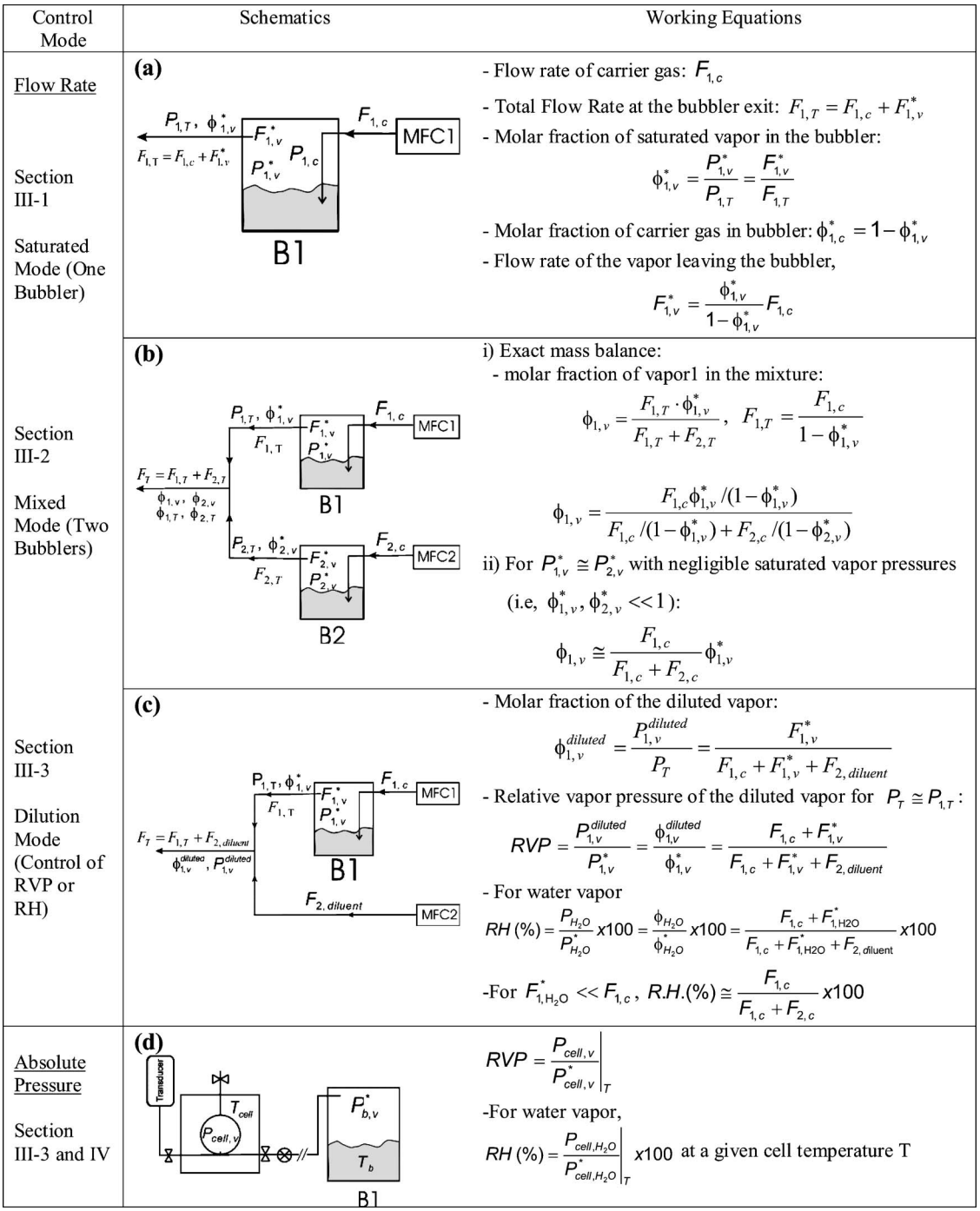

FIG. 4. Summary of working equations for *in situ* vapor sorption apparatus.

$$\phi^{\text{diluted}}_{1,v} = \frac{\phi^*_{1,v} F_{1,c}/(1-\phi^*_{1,v})}{F_{1,c}/(1-\phi^*_{1,v}) + F_{2,\text{diluent}}}. \tag{8}$$

In the instance when the vapor pressure is very small (i.e., $\phi^*_{1,v} \ll 1$), Eq. (8) simplifies to

$$\phi^{\text{diluted}}_{1,v} \approx \frac{\phi^*_{i,v} F_{1,c}}{F_{1,c} + F_{2,\text{diluent}}}. \tag{9}$$

The relative vapor pressure (RVP) is defined as

$$\text{RVP} = \frac{P^{\text{diluted}}_{1,v}}{P^*_{1,v}} = \frac{\phi^{\text{diluted}}_{1,v} P_T}{\phi^*_{1,v} P_{1,T}} = \frac{F_{1,c} + F^*_{1,v}}{F_{1,c} + F^*_{1,v} + F_{2,\text{diluent}}} \frac{P_T}{P_{1,T}}, \tag{10}$$

and in the case where the vapor pressure is small (i.e., $\phi^*_{1,v} \ll 1$) and the pressure drop between the bubbler and the cell is small (i.e., $P_T \cong P_{1,T}$) (see the Appendix), RVP can be simplified to

$$\text{RVP} \cong \frac{F_{1,c}}{F_{1,c} + F_{2,\text{diluent}}}. \tag{11}$$

If the vapor is water, the RVP can be expressed as RH,

$$\mathrm{RH} = \mathrm{RVP} \times 100\,\% = \frac{P_{\mathrm{H_2O}}^{\mathrm{diluted}}}{P_{\mathrm{H_2O}}^{*}} \times 100\,\% \,. \tag{12}$$

Using the same assumptions as for Eq. (12), the RH can be approximated as follows:

$$\mathrm{RH} \cong \frac{F_{1,c}}{F_{1,c} + F_{2,\mathrm{diluent}}} \times 100\,\% \,. \tag{13}$$

2. Absolute pressure control

In this mode of operation, the RVP in the sample cell is controlled by controlling the absolute pressure in the cell at a fixed temperature with a vacuum pump, manometer, and programmable control valve.[11] This method involves controlling the absolute pressure in the cell by actively controlling the opening in the control valve at the upstream side, and by manually adjusting the metering valve at the downstream side of the sample cell. The sample cell and the vapor delivery tubing must be evacuated, and liquid in the bubbler must be degassed before operating in this mode. Since this method controls the absolute pressure P_v (i.e., P_{cell}) of pure vapor in the cell, a desired RVP can be directly obtained from the RVP definition without any assumptions,

$$\mathrm{RVP} = \left.\frac{P_v}{P_v^*}\right|_T = \left.\frac{P_{\mathrm{cell}}}{P_{\mathrm{cell},v}^*}\right|_T , \tag{14}$$

where P_v^* and $P_{\mathrm{cell},v}^*(T)$ are saturated pure vapor pressures, at a given temperature, which can be obtained from the literature. RH in the sample cell is given by

$$\mathrm{RH} = \left.\frac{P_{\mathrm{cell,H_2O}}}{P_{\mathrm{cell,H_2O}}^*}\right|_T \times 100\,\% \,. \tag{15}$$

The saturated vapor pressure $P_{\mathrm{cell,H_2O}}^*(T)$ of water can be obtained from the literature.[12] The following is the result of fitting the data over the range of −15 °C–150 °C:

$$\begin{aligned} P_{\mathrm{cell,H_2O}}^*(^\circ\mathrm{C}) = &-2.9902 \times 10^{-11} T^6 + 2.8571 \times 10^{-8} T^5 \\ &+ 1.3731 \times 10^{-6} T^4 + 2.2334 \times 10^{-4} T^3 \\ &+ 1.0617 \times 10^{-2} T^2 + 3.2786 \times 10^{-1} T \\ &+ 4.6004 \quad (\chi^2 = 2.4497), \end{aligned} \tag{16}$$

where T is in °C and $P_{\mathrm{cell,H_2O}}^*(T)$ in mm Hg.

IV. RH CONTROL

The conventional way to control RH is to use a saturated salt solution for a desired humidity range. Although this method is accurate, changing saturated salt solutions to change the RH may not be simple. Also, it takes a long time to reach the saturated vapor pressure depending on the headspace size. Also, if the salt solution is not handled with care, it may contaminate the sample. Here, the RH in the sample cell is controlled as discussed in Sec. III C (i) by adjusting both the flow rate of the carrier gas for solvent reservoir, B1, and that for the dry diluent gas, or (ii) by controlling the absolute pressure in the cell at a given temperature. The performance of the *in situ* vapor sorption apparatus for controlling the RH was evaluated, focusing on accuracy, stability, and response time. The results are discussed below.

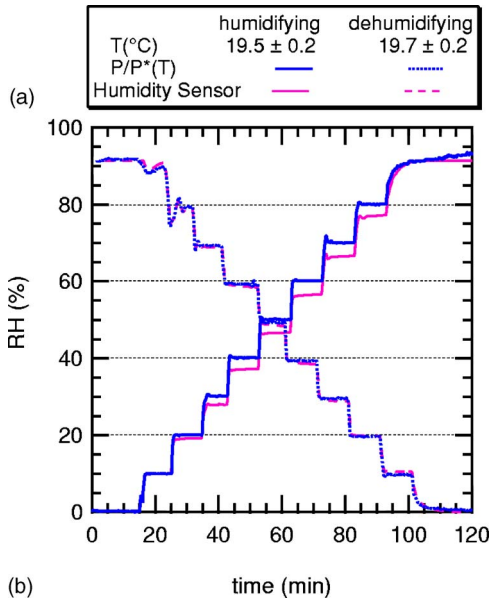

FIG. 5. Stepwise RH (with 10% RH interval) increment (a) with simultaneous measurement of RH during humidifying (solid line) and dehumidifying (dotted line) with the transducer (blue) and humidity sensors (pink) in the cell at 20 °C and corresponding pressure (b) increment. [The humidity sensor was calibrated with a saturated (or wet) salt solution. The RH (pink) from the humidity sensor reading above 90% RH out of range before calibration, which shows a constant value. Therefore the values above 90% RH from the humidity sensor is not correct].

A. Accuracy

The accuracy of pressure control was tested by making stepwise pressure increments at 10 min intervals (Fig. 5), which corresponded to around 10% changes in the RH. Only near saturation, i.e., above 2 kPa (i.e., 15 mm Hg, and RH ≈85% at 20 °C), does the pressure fluctuate before stabilizing. (This fluctuation can be reduced by increasing the amount of saturated vapor in the vapor delivery line). Except for this extreme condition, the accuracy depends only on the accuracy of the pressure transducer, which is 0.5% of its reading according to the manufacturer. The accuracy includes nonlinearity, hysteresis, and nonrepeatability.[13]

The reliability of the pressure control method was confirmed by comparing the relative humidity from the pressure measurement with a secondary standard such as a calibrated humidity sensor.[14] For this comparison, pressure, relative humidity, and temperature in the cell were measured simultaneously every 10 s. In order to minimize the error due to small temperature fluctuations in the cell, the saturated vapor pressures were calculated at each corresponding temperature with Eq. (16) rather than using a mean temperature. The humidity sensor shows hysteresis during the cycle. The difference between the two measurements of RH is about 5% RH during humidifying, but is negligible on drying (Fig. 5).

Controlling humidity by this method requires opening the metering valve to a predetermined position, depending on the target vapor pressure, and then restricting the degree of opening allowed for the control valve. These precautions are

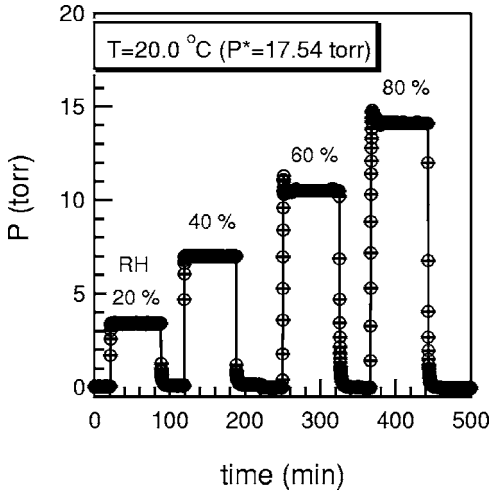

FIG. 6. Pressure jump to reach to the indicated target humidity starting from $P \sim 0.0$ Torr at 20 °C. The pressure is recorded in 10 s intervals (1.000 Torr can be converted to 133.3 Pa).

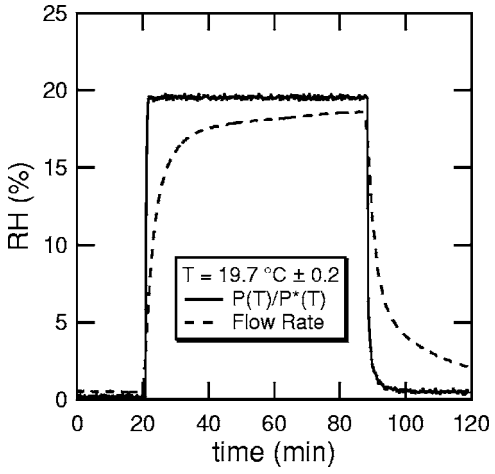

FIG. 7. Comparison of pressure control method and flow rate control method to reach 20% RH.

necessary to avoid, particularly at high RH, large pressure excursions caused by the relatively slow response of the control valve.

B. Response time and stability

The response time to reach 90% of a target RH was measured starting from $P \approx 0.0$ Pa (Fig. 6). In the RH range of 0%-80%, the response time to reach the target pressure is less than 1–2 min without any significant overshoot. To reach a RH of 80%, there is a 5% overshoot, and it takes around 10 min for the pressure to stabilize. This overshoot can be minimized by using a gradual pressure increase after reaching 90% of the target pressure. The current humidity control method takes less than 1–2 min to reach 90% ($t90$) of the target RH regardless of target humidity. Minimizing the response time is important to study the initial structure change of the materials under a vapor environment as well as to study diffusion kinetics.

C. Comparison of two methods

As described in the previous section, RH can also be controlled by mixing a saturated vapor with a diluent gas [Eqs. (12) and (13)], and the response time and stability of this method was also evaluated. As shown in Fig. 7, the flow rate control method (FRCM) shows a long response time to reach 20% RH, as much as $t90=40$ min with a total flow rate=10.0 SCCM compared to $t90 \approx 40$ s with the pressure control method. Also, there is an approximately 2 min induction time before the FRCM shows a sensor response. The long response time in the flow mixing method can be reduced with higher capacity MFCs. Both methods are stable once the target relative humidity is reached, but there is a difference of as much as 5% RH between the two methods. The flow rate mixing method shows slightly lower RH ($\approx 1\%$ RH) compared to pressure measurement as shown in Fig. 7. This may be due to the humidity sensor hysteresis or incomplete saturation of the carrier gas. The flow rate mixing method sometimes showed an overshoot and a long dehumidifying process. This is due to the water vapor condensate accumulated in the vapor delivering tube and volume ballast mixer when the saturated carrier gas was used for a long time. When the line was used below saturated condition, these problems were not observed. Unlike the flow rate control method, pressure control is not affected by condensation, because only a controlled amount of vapor is allowed to flow into the cell. In fact, in pseudoclosed operation, the condensation in the tube helps to reach the target humidity in the cell much faster than reported here. For example, to reach RH > 85% at 22 °C, it takes around 1.5 min with heating the bubbler at 35 °C and the vapor delivering tube at ≈27 °C. Both methods are compared in Table I.

D. Control of organic solvent vapor pressure

In addition to controlling water vapor, which has low vapor pressure and strong hydrogen bonding, the *in situ* vapor sorption apparatus can control an organic vapor with

TABLE I. Comparison of pressure control (PCM) and flow rate control method (FRCM).

	PCM	FRCM[a]
Response time	Negligible (<1–2 min)	>30 min
Overshoot	Due to valve response	Due to condensed vapor in tubing
Stability	Stable over hours	Stable over hours
Operation	Complex	Simple
Process variable	Absolute pressure	Flow rate of carrier gas
Uncertainty	Temperature	Temperature, liquid water level in bubbler

[a]Flow rate of 1.67×10^{-7} m^3/s (i.e., 10 SCCM).

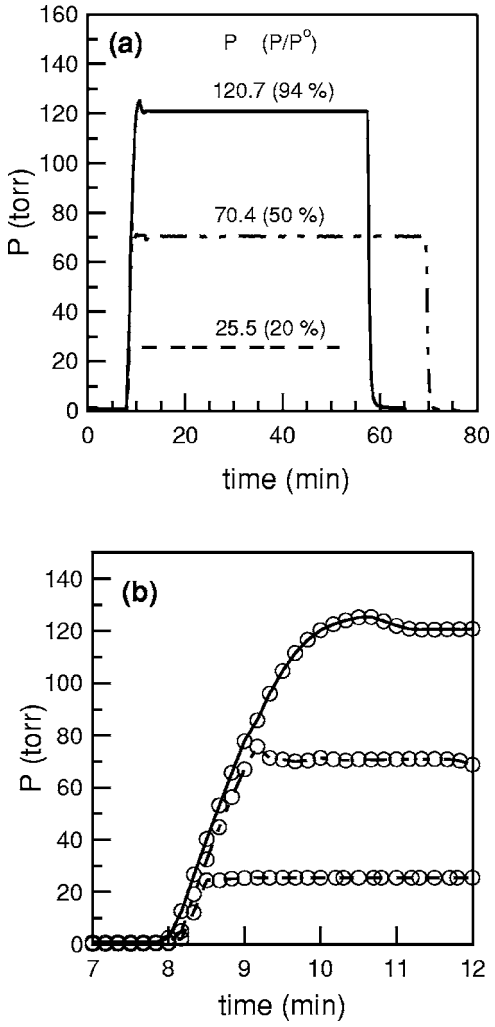

FIG. 8. (a) Pressure jump profile of deuterated *n*-hexane; (b) response time to reach the indicated target pressure during sorption time of semicrystalline linear PE.

weak van der Waals interaction and high vapor pressure. Figure 8 shows the response time to reach to various target pressures of deuterated *n*-hexane. The response time to reach a relative pressure (P/P^o) of 95% from 0% is approximately 2 min [Fig. 8(b)], and reaching a lower target relative pressure takes 1–2 min. Pressure fluctuation with time is negligible (±0.05%). The results suggest that the apparatus can control RH and RVP accurately within 1% error range.

E. Uncertainty of RH from both methods

Knowing the temperature inside the cell is important to convert pressure to RH. Temperature uncertainty originated from the use of multiple, physically separated heat sources rather than temperature fluctuations. Currently, the temperature of the cell is measured on its outside surface. The difference between the inside and outside temperature at a 40.0 °C bath temperature is ≈1.0 °C, and the difference depends on the temperature range and the surrounding temperature. Also the pressure transducer temperature is controlled by an independent heat source causing another uncertainty. At room temperature, these temperature-related uncertainties were negligible. But at temperatures other than room temperature, the uncertainty of the relative humidity due to temperature differences must be considered.

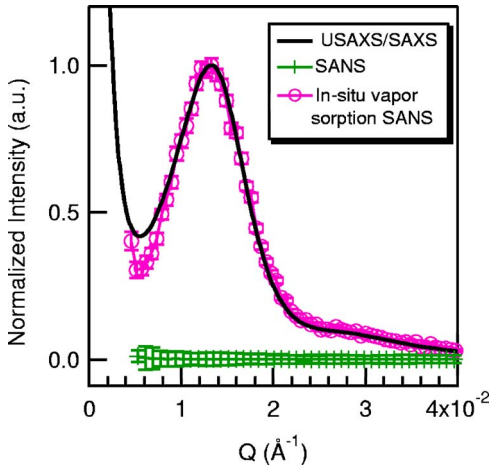

FIG. 9. Comparison of synchrotron USAXS/SAXS (solid line), SANS (cross), and *in situ* vapor sorption SANS (circle) of melt-crystallized linear polyethylene at 110 °C. *In situ* vapor sorption SANS was obtained with 5 min sorption and 1 min SANS run at 95% relative vapor pressure of deuterated *n*-hexane at 21 °C. The intensity was matched in the peak height and peak position. The SAXS peak was shifted to SANS peak by ≈1.2×10^{-3} Å. (Solid line and cross for the dry and circle for the wet polyethylene.)

V. RESULTS

The utility of the *in situ* vapor sorption apparatus depends on the assumption that an appropriate vapor can selectively penetrate into materials with different structural domains. The sorbed vapor can change the contrast between domains depending on the scattering length density of the vapor and domains. We present preliminary SANS results obtained using (i) the relative vapor pressure control method and (ii) the vapor flow rate control method to demonstrate the concept experimentally and to provide some ideas for future experiments.

The application and performance of the *in situ* vapor sorption apparatus were tested with various materials with

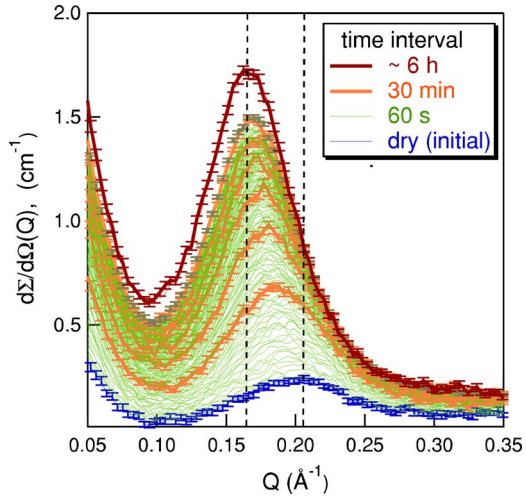

FIG. 10. Structure evolution in ionic group of Nafion112 with H_2O wetting time with a flow rate control (5 SCCM).

TABLE II. Pressure drops (ΔP) with various liquids and vapors, considering (i) the length and inner diameter of the vapor delivery tube, and (ii) the elevation difference between the cell at the SANS beam and the bubblers with a flow rate of 10 SCCM.

Flow rate (F)	1.67×10^{-7} m^3/s
Tube length (L)	2.44 m
Inner diameter (Di)	1.59×10^{-3} m
Elevation change (Δh)	0.31 m
Cross area (A)	1.979×10^{-6} m^2
Linear velocity (v)	0.084 m/s
Acceleration of gravity (g)	9.807 m/s^2
Inner surface roughness (neglected)	

Liquid	*Density*	*Newtonian viscosity*	*Reynold number*[a]	*Pressure drop*
	ρ(g/cm3)	μ(Pa s)	Re	ΔP(Torr)
n-hexane	0.66	4.50E-04	195.7	23.6
Toluene	0.87	5.88E-04	196.6	30.9
Water	1.00	1.00E-03	133.7	42.0
Vapor/gas				
Water vapor at 100 °C	5.90E-04	1.20E-05	6.6	0.25
Water vapor at 20 °C	1.73E-05	1.00E-05	0.2	0.20
Air at 20 °C	1.29E-03	1.80E-05	9.4	0.39
N_2 at 0 °C	1.25E-03	1.73E-05	9.6	0.37

[a]$\mathrm{Re}=\rho v D/\mu$.

different structures: (i) semicrystalline polyolefin to demonstrate contrast enhancement due to preferred wetting of the amorphous phase in a semicrystalline system[15] with the absolute pressure control, and (ii) a Nafion112 polyelectrolyte membrane with the flow rate contol, focusing on the water vapor control ability of the apparatus:

(i) The SANS results for a linear polyethylene (PE) sample (thickness: 100 μm$\pm$1 μm) crystallized isothermally at 110 °C from the melt shows very weak scattering despite the mass density difference between the crystalline and amorphous regions, while small-angle x-ray scattering (SAXS) shows a strong scattering peak as shown in Fig. 9. The null SANS scattering of the semicrystalline PE is due to the similar scattering length density (SLD) between crystalline and amorphous phases. A square of the neutron SLD difference $(\Delta\mathrm{SLD})^2_{\mathrm{Neutron}}$ between the two phases is three orders of magnitude smaller than the $(\Delta\mathrm{SLD})^2_{\mathrm{X\ ray}}$ for x rays. When the sample was exposed to a contrast-generating vapor (for example, deuterated hexane) using the *in situ* vapor sorption apparatus, the scattering peak started to appear within a few minutes. Figure 9 shows an example (5 min sorption and 1 min SANS run) of the SANS scattering profiles collected during vapor (deuterated *n*-hexane) sorption at the relative vapor pressure of 95% at 21 °C.[16] This demonstrates that most of the vapor selectively wets the amorphous phase. The quality of the SANS data is comparable to that of synchrotron SAXS. For comparison, peak intensities were matched in height and position. The peak profiles are nearly identical, which demonstrates that SANS can be used for studying the structure of semicrystalline polymers without using deuterated polymers.

(ii) The apparatus has the capability of controlling water vapor, which has hydrogen bonding and low vapor pressure as well as mixing D_2O/H_2O vapor for contrast matching experiments. As-received Nafion112 (extruded) was initially dried under vacuum at RT in the vapor sorption cell and wet by H_2O vapor (Fig. 10). The SANS intensity was collected in 60 s intervals and shows a large intensity increase with sorption time as well as a peak position shift from $Q=0.21$ to 0.165 $\mathrm{Å}^{-1}$ that corresponds to a *D*-spacing change from 29.9 to 38.1 Å. This average spacing between ionic domains, as well as the sorption isotherm, diffusion coefficient, and correlation between the structure and vapor diffusion can be investigated with sorption time. Quantitative results will be given elsewhere.

VI. DISCUSSION

The initial version of a multipurpose *in situ* vapor sorption apparatus has been built for SANS experiments. The apparatus can effectively (i) control the vapor pressure or relative humidity by controlling pressure or flow rate, (ii) mix two H/D vapors continuously for contrast matching SANS experiments, and (iii) allow for injection of a liquid to the cell under vacuum. A target humidity (or vapor pressure) can be reached in less than 1–2 min using the pressure control method. Preliminary experimental results show that the apparatus is effective for studying the structure of semicrystalline polymers, and polyelectrolyte membranes. The apparatus requires only a single sample for experiments on contrast variation and sorption/desorption kinetics.

ACKNOWLEDGMENTS

This work was partially supported by NSF (DMR-9986442). The authors wish to thank the NCNR technical staff, namely, Scott Slifer for his dedicated contribution in building the apparatus, James LaRock for cell design, Nick Maliszewskyj's group for electrical wiring, and Dan Dander's sample environment group for leak testing. The authors also thank Barry Bauer, Christopher Soles, and Ron Hedden of NIST's Polymers Division for sharing their experience, Jeff Anderson of the Fabrication Technology Division for the bubbler design, Peter H. Huang of NIST's Process Measurements Division for reviewing the manuscript, and especially J. David Londono for the synchrotron SAXS experiment. The synchrotron SAXS work was performed at the DuPont-Northwestern-Dow Collaborative Access Team (DND-CAT) Synchrotron Research Center located at Sector 5 of the Advanced Photon Source. DND-CAT is supported by the E.I. DuPont de Nemours & Co., The Dow Chemical Company, the U.S. National Science Foundation through Grant No. DMR-9304725 and the State of Illinois through the Department of Commerce and the Board of Higher Education Grant No. IBHE HECA NWU 96. Use of the Advanced Photon Source was supported by the U.S. Department of Energy, Basic Energy Sciences, Office of Energy Research under Contract No. W-31-102-Eng-38.

APPENDIX: PRESSURE DROP

When there is a pressure drop between the bubbler and sample cell position, it is difficult to reach a saturated vapor pressure. In the FRCM, the vapors flow from the bubblers to the sample cell along with a long tube [$L/D=3072$ (o.d. $=3.26\times10^{-3}$ m, i.d. $\approx1.6\times10^{-3}$ m, length $L\approx2.44$ m tube ignoring the valve joints], having an elevation change, $\Delta h(=h_B-h_{SC})$, between the bubbler (h_B) and sample cell compartment (h_{SC}). The Reynold numbers of various vapors that were calculated at a maximum flow rate of 1.67×10^{-7} m^3/s (10 SCCM) of the MFC are small ($Re\ll2100$), which implies the flow in the tube is laminar. A pressure drop in the pipe with a laminar flow (i.e., Hagen-Poisseuille) can be expressed[17]

$$\Delta P=\frac{\bar{\rho}v^2L}{2D_i}\frac{64}{\mathrm{Re}}+\bar{\rho}g\Delta h \quad \left(\text{or } \Delta P=\frac{\bar{\rho}v^2L}{D_i}2f+\bar{\rho}g\Delta h, f=16/\mathrm{Re}\right) \quad \text{for } \mathrm{Re}<2100, \tag{A1}$$

which is proportional to the mass density ($\bar{\rho}$,kg/m^3) of vapor, a square of vapor linear velocity (v,m/s), L/D_i ratio of the tube, and elevation change Δh. The calculated pressure drop, $\Delta P(=P_B-P_{SC})$, between the bubbler and the sample cell is summarized in Table II for the liquid and vapor/gas. The pressure drop for the vapors is less than 67 Pa (0.5 Torr). Although this small pressure drop does not affect the apparatus performance in FRCM, it prohibits direct measurement of saturated vapor pressure. The maximum target RVP (or RH) is approximately 93%–95%.

[1] E. Hoinkis, Langmuir **12**, 4299 (1996).
[2] R. C. Hedden, H.-J. Lee, and B. J. Bauer, Langmuir **20**, 416 (2004).
[3] C. Soles, H.-J. Lee, E. K. Lin, and W.-I. Wu, NIST Spec. Publ. **960-13**, 1-58 (2004).
[4] S. D. Hersee and J. M. Ballingall, J. Vac. Sci. Technol. A **8**, 800 (1990).
[5] E. Kondoh and T. Ohta, J. Vac. Sci. Technol. A **13**, 2863 (1995).
[6] S. N. Dhoot and B. D. Freeman, Rev. Sci. Instrum. **74**, 5173 (2003).
[7] S. Hasegawa and J. W. Little, J. Res. Natl. Bur. Stand., Sect. A **81**, 81 (1977).
[8] *Humidity and Moisture, Measurement and Control in Science and Industry*, edited by A. Wexler and W. A. Wildhack (Reinhold, New York, 1963), Vol. 3.
[9] Certain commercial equipment, instruments, or materials are identified in this paper to foster understanding. Such identification does not imply recommendation or endorsement by the National Institute of Standards and Technology, nor does it imply that the materials or equipment identified are necessarily the best available for the purpose.
[10] $P_{1,T}$ is approximately atmospheric pressure $P_{1,T}=P_{air}+P^*_{1,v}\cong10^5$ Pa (760 mm Hg) in the open-loop operation. In the case that there is no carrier gas flow (i.e., $F_{1,c}=0$), $\phi^*_{1,v}$ of Eq. (1) does not become one because the carrier gas term of Eq. (1) is replaced with an air flow rate F_{air} and air partial pressure P_{air}. The $\phi^*_{1,v}$ becomes one only in the closed loop operation after degassing the liquid in the bubbler.
[11] Also, it is possible to control RVP by adjusting the temperature of the cell. In this case, the response time to reach a target pressure depends on the heating/cooling rate.
[12] *CRC Handbook of Chemistry and Physics*, 65th ed., edited by R. C. Weast (CRC, Boca Raton, FL, 1984).
[13] MKS Instruction Manual.
[14] A commercial humidity sensor [HC-610] was calibrated at room temperature with saturated salt solutions of sodium chloride (RH=75.4%), potassium carbonate (RH=43.2%), and a wet salt of magnesium chloride (RH=32.8%) as follows: the humidity sensor was placed in a 500 mL plastic bottle containing a wet salt dispersed on the bottom, and the RH was recorded with time. The RH reading was recorded until it became constant for approximately one day.
[15] M.-H. Kim and C. J. Glinka, J. Appl. Crystallogr. **38**, 734 (2005).
[16] Relative vapor pressure of the deuterated *n*-hexane ($P=16.079$ kPa) was estimated with a saturated vapor pressure ($P^*=16.905$ kPa) of protonated *n*-hexane at 21 °C.
[17] R. B. Bird, W. E. Stewart, and E. N. Lightfoot, *Transport Phenoma* (Wiley, New York, 1960).